

# Protein conformational changes and protonation dynamics probed by a single shot using quantum-cascade-laser-based IR spectroscopy

Cite as: J. Chem. Phys. **156**, 204201 (2022); <https://doi.org/10.1063/5.0088526>

Submitted: 17 February 2022 • Accepted: 29 April 2022 • Published Online: 26 May 2022

 Luiz Schubert, Pit Langner, David Ehrenberg, et al.

## COLLECTIONS

Paper published as part of the special topic on [Time-resolved Vibrational Spectroscopy](#)



View Online



Export Citation



CrossMark

## ARTICLES YOU MAY BE INTERESTED IN

[Femtosecond-to-millisecond mid-IR spectroscopy of photoactive yellow protein uncovers structural micro-transitions of the chromophore's protonation mechanism](#)

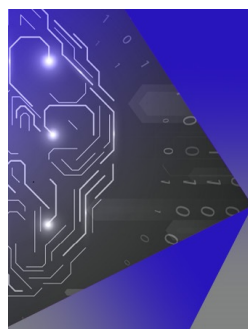
The Journal of Chemical Physics **156**, 205103 (2022); <https://doi.org/10.1063/5.0091918>

[Polaritonic effects in the vibronic spectrum of molecules in an optical cavity](#)

The Journal of Chemical Physics **156**, 204119 (2022); <https://doi.org/10.1063/5.0089412>

[Resonance conditions, detection quality, and single-molecule sensitivity in fluorescence-encoded infrared vibrational spectroscopy](#)

The Journal of Chemical Physics **156**, 174202 (2022); <https://doi.org/10.1063/5.0088435>



## APL Machine Learning

Machine Learning for Applied Physics  
Applied Physics for Machine Learning

**First Articles  
Now Online!**

# Protein conformational changes and protonation dynamics probed by a single shot using quantum-cascade-laser-based IR spectroscopy

Cite as: J. Chem. Phys. 156, 204201 (2022); doi: 10.1063/5.0088526

Submitted: 17 February 2022 • Accepted: 29 April 2022 •

Published Online: 26 May 2022



View Online



Export Citation



CrossMark

Luiz Schubert,<sup>1</sup>  Pit Langner,<sup>1</sup> David Ehrenberg,<sup>1</sup> Victor A. Lorenz-Fonfria,<sup>2</sup>  and Joachim Heberle<sup>1,a)</sup> 

## AFFILIATIONS

<sup>1</sup> Experimental Molecular Biophysics, Department of Physics, Freie Universität Berlin, Arnimallee 14, 14195 Berlin, Germany

<sup>2</sup> Institute of Molecular Science, Universitat de Valencia, Catedrático José Beltrán Martínez, No. 2, 46980 Paterna, Spain

**Note:** This paper is part of the JCP Special Topic on Time-Resolved Vibrational Spectroscopy.

**a) Author to whom correspondence should be addressed:** joachim.heberle@fu-berlin.de. Tel.: +49-30-838-56161

## ABSTRACT

Mid-IR spectroscopy is a powerful and label-free technique to investigate protein reactions. In this study, we use quantum-cascade-laser-based dual-comb spectroscopy to probe protein conformational changes and protonation events by a single-shot experiment. By using a well-characterized membrane protein, bacteriorhodopsin, we provide a comparison between dual-comb spectroscopy and our homebuilt tunable quantum cascade laser (QCL)-based scanning spectrometer as tools to monitor irreversible reactions with high time resolution. In conclusion, QCL-based infrared spectroscopy is demonstrated to be feasible for tracing functionally relevant protein structural changes and proton translocations by single-shot experiments. Thus, we envisage a bright future for applications of this technology for monitoring the kinetics of irreversible reactions as in (bio-)chemical transformations.

© 2022 Author(s). All article content, except where otherwise noted, is licensed under a Creative Commons Attribution (CC BY) license (<http://creativecommons.org/licenses/by/4.0/>). <https://doi.org/10.1063/5.0088526>

## INTRODUCTION

Understanding protein dynamics is of fundamental importance to study the function of proteins. A sophisticated theoretical and experimental biophysical toolbox has been developed over the years to gain insight into the relationship between function and structural rearrangements.<sup>1</sup> Among those, vibrational spectroscopy offers a label-free way to access not only alterations in the secondary structure of a protein but also ligand binding, co-factor changes, or even proton transfer reactions by analysis of Fourier-transform infrared (FTIR) difference spectra.<sup>2</sup> To observe sub-ms dynamics of protein function over a broad spectral range, time-resolved step-scan FTIR spectroscopy was developed.<sup>3</sup> Despite its success, the use of step-scan has remained limited to a restricted number of mostly light-activatable proteins. One reason is that this technique requires stable proteins with a repetitive photoreaction, preferably with a recovery faster than a second. Longer recoveries render step-scan spectroscopic studies very challenging and close to impossible for probing irreversible processes.<sup>4,5</sup>

Numerous attempts to overcome the limitations of time-resolved step-scan FTIR spectroscopy while retaining the benefits of its wide spectral range have been made by employing different strategies. With a fast scanning interferometer, the time for recording a full IR spectrum was improved from the ms range to the  $\mu$ s range. However, due to the low emission of globars—the typical light source of FTIR spectrometers—many repetitions had to be made to achieve an averaged spectrum with an adequate signal-to-noise ratio (SNR).<sup>6</sup> It is conceptually possible with time-resolved multiple-probe spectroscopy (TRMPS) to record mid-IR spectra with a spectral bandwidth of hundreds of  $\text{cm}^{-1}$  and a temporal resolution given by the repetition frequency of the probing broadband IR pulsed laser, e.g., 10  $\mu$ s for a 100 kHz laser. In practice, however, the sample needs to be repeatedly excited, both to achieve sufficient SNR by data averaging and to improve the temporal resolution down to picoseconds by collecting spectra at variable optical delays.<sup>7,8</sup> Recently, a novel dispersive IR spectrometer using highly brilliant synchrotron radiation succeeded to record spectra between 1800 and 1000  $\text{cm}^{-1}$  of bovine rhodopsin at  $\mu$ s time resolution,

averaging only seven single-shot experiments for obtaining sufficient SNR.<sup>9</sup> Although promising, this approach is not easily transferable to a table-top machine. In contrast, scanning spectrometers using tunable external cavity quantum cascade lasers (EC-QCLs) are technically less complex. The intense QCL emission provides a high photon flux and, therefore, allows us to achieve sufficient SNR already on the ns time scale. However, the monochromatic QCL emission must be tuned in frequency to retrieve spectral information.<sup>10</sup> Dual-comb spectroscopy (DCS), on the other hand, is an elegant table-top approach to circumvent the technical limitations introduced by interferometers or dispersive elements. This multiplex technique uses the high photon output of QCLs and a heterodyne detection scheme to provide spectro-temporal data with each acquisition.<sup>11,12</sup> DCS provides data of sufficient SNR to observe the retinal isomerization in bacteriorhodopsin (bR) as well as GTP hydrolysis in Ras proteins by single- or ten-shot experiments, respectively.<sup>12,13</sup> Yet, its application is often limited by the availability of suitable laser systems with emissions in the desired spectral range of the experiment.

In this study, we used bacteriorhodopsin (bR) as a model protein of integral membrane proteins to scrutinize various advantages and disadvantages of a commercially available dual-comb spectrometer in comparison to our homebuilt EC-QCL spectrometer.<sup>10</sup> bR was chosen because it represents a photoactivatable protein that exhibits relevant structural changes and protonation dynamics in the micro- to millisecond time range. The light-induced structural changes of this proton pump give rise to IR difference spectra. Most of the difference bands have been assigned to molecular vibrations of the chromophore, protein backbone, or even to single amino acid side chains.<sup>14</sup> In bR, light activation leads to net proton transport from the cytoplasmic to the extracellular side. This vectorial transport is achieved by a sequence of thermal reactions after the initial photoreaction [Figs. 1(a) and 1(b)]. In this mechanism, protonation of D85 and reprotonation of the retinal Schiff base (RSB) by D96 [Fig. 1(c), steps 1 and 3, respectively] are crucial steps elucidated by FTIR spectroscopy.<sup>14</sup> Protonation of D85 is reflected by a positive band centered at  $1761\text{ cm}^{-1}$  upon formation of the M intermediate [Fig. 1(c), step 1], which shifts toward  $1755\text{ cm}^{-1}$  during the transition to the N intermediate. This shift is caused by a change in the hydrogen bonding due to a structural change at helix C [Figs. 1(c) and 1(d)].<sup>15</sup> Deprotonation of D96, which leads to proton transfer to the RSB during the lifetime of the N intermediate [Fig. 1(c), step 3], is reflected by a negative band centered at  $1742\text{ cm}^{-1}$ .<sup>16</sup>

Here, we present the first DCS experiment carried out in the amide I region ( $1680\text{--}1620\text{ cm}^{-1}$ ), probing protein conformational dynamics, as well as in the carboxylic C=O region ( $1770\text{--}1720\text{ cm}^{-1}$ ), reporting on H-bonding and protonation changes of Asp and Glu side chains. The applicability of single-shot experiments is demonstrated and compared to a QCL-based scanning spectrometer that provides transients at single frequencies. Our results showcase a novel spectroscopic method to study conformational and protonation dynamics that finally aim at studies of transmembrane receptors including ligand-gated ion channels, G protein-coupled receptors, and hormone receptors. This technique opens the door toward time-resolved studies revealing mechanistic details of irreversible (bio-)chemical reactions when an educt is transformed into a product.

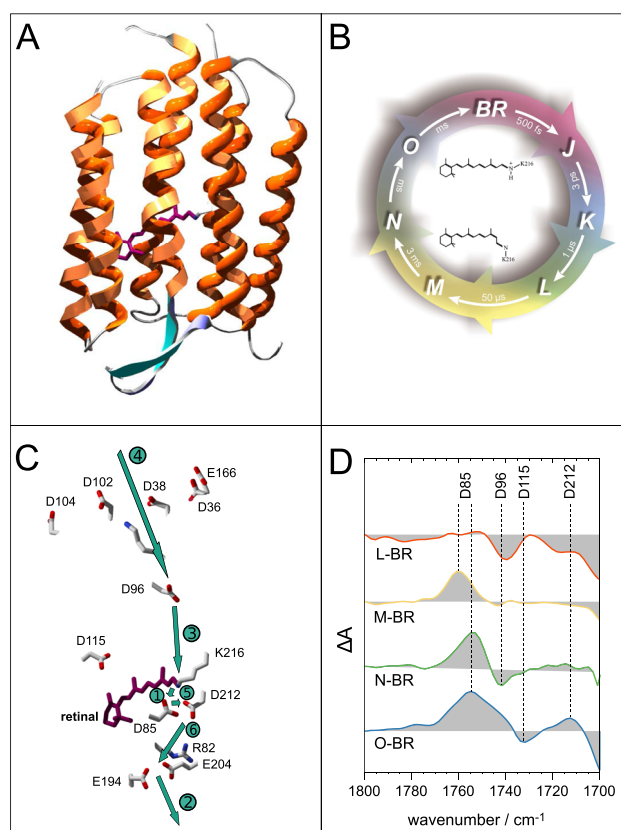


**FIG. 1.** Overview of the cyclic photoreaction of bacteriorhodopsin. [Reproduced with permission from Radu *et al.*, Photochem. Photobiol. Sci. **8**, 1517 (2009). Copyright 2009 The European Photochemistry Association and The Royal Society of Chemistry.] (a) Structure of bacteriorhodopsin. (b) Photocycle scheme of bR. After ultrafast photoisomerization from all-*trans* to 13-*cis* retinal, a sequence of thermal reactions occurs involving K, L, M, N, and O intermediate states. Time constants of the rises of the intermediate states are indicated by the arrows. (c) Sequence of protonation steps as indicated by green arrows and numbering. (d) Step-scan FTIR difference spectra in the carboxylic acid range. Proton transfer from the retinal Schiff base to D85 (step 1) is reflected by a positive band at  $1761\text{ cm}^{-1}$ . D85 remains protonated until recovery of ground-state bR but changes the hydrogen bonding in the N and O intermediates as reflected by spectral redshifts.

## MATERIALS AND METHODS

### Sample preparation

The light-driven proton pump bacteriorhodopsin (bR) has been prepared from *Halobacterium salinarum* strain S9 as previously described.<sup>17</sup> Purple membrane patches containing bR were dispersed in a low-ionic strength buffer containing 2 mM HEPES and 2 mM NaCl at a pH of 7.4. Several  $\mu\text{l}$  of the protein solution were dried on a BaF<sub>2</sub> window under a gentle stream of dry air. Subsequently, the protein film was rehydrated over the vapor phase by placing 4  $\mu\text{l}$  of a water/glycerol mixture (8:2 wt./wt.) next to the protein film. Sufficient rehydration was confirmed by monitoring the protein amide and the water absorption bands with a Bruker Vertex 80v FTIR spectrometer.

## Quantum cascade laser spectroscopy

Time-resolved dual-comb spectroscopy was conducted with a commercially available dual-frequency-comb spectrometer (IRsweep IRis-F1) as described elsewhere.<sup>12,13</sup> Briefly, the emission of two QCL frequency combs are overlaid on a 50:50 CaF<sub>2</sub> beamsplitter and attenuated with neutral density filters. One combined beam is focused on an MCT detector as a reference, while the other beam is transmitted through the sample. A fast-Fourier transform algorithm is applied to the heterodyne beating signal, with an integration time defining the time resolution of the measurements. Although the use of sub- $\mu$ s integration times has been demonstrated<sup>12</sup>, we used an integration time of 4  $\mu$ s to increase the SNR.

The spectral coverage depends on the spectral overlap of the two frequency combs, which constitute the laser module of the spectrometer. Here, two different laser modules have been used. For analysis in the amide I region we used a module providing a spectral bandwidth of 1680–1620 cm<sup>-1</sup>, and for the carboxylic region a module providing a spectral coverage of 1770–1720 cm<sup>-1</sup>.

In DCS, the spectral resolution is given by the inherent spacing of the comb lines. To improve the signal-to-noise ratio (SNR), adjacent comb lines were averaged by using a Python script provided by IRsweep, resulting in a spectral resolution of  $\sim 4.5$  cm<sup>-1</sup> (for 3000 shots experiments) or of 8.1 cm<sup>-1</sup> (for single-shot experiments). In a conventional moving average smoothing,  $n$  neighboring lines on each side of the central line are averaged, with the final spectral resolution given by  $(2n + 1) \times f_{REP}$ , with  $f_{REP}$  being the comb line spacing (here  $\sim 0.3$  cm<sup>-1</sup>). However, the intensity of individual laser lines in DCS varies substantially from each other, and so does their noise level. To account for this, the spectral smoothing conducted by the IRsweep software employs a weighted moving average, with the points around a central line being weighted by the inverse of its noise variance ( $1/\sigma^2$ ). The standard deviation of the noise for each laser line ( $\sigma$ ) was derived from the fluctuations of the pretrigger data points in a time-resolved experiment.

Time-resolved scanning laser IR spectroscopy was carried out using our homebuilt external cavity QCL setup.<sup>10</sup> Briefly, a frequency tunable external cavity quantum cascade laser (QCL1: MIRcat-1100-U3 QCL2: TLS41058, Daylight Solutions, San Diego, USA) was used as a monochromatic light source, in continuous wave mode. In this setup, once a new wavenumber is selected, the light intensity reaching the detector is monitored and the beam is attenuated appropriately to avoid saturation of the detector. The attenuated IR beam passes the sample and is focused on the MCT detector (KV104-0.5-A3/11, Kolmar Tech, Inc.). The signal is digitized by two oscilloscopes (Picoscope 4227, Pico Technology) at high (250 MS/s) and low (1 MS/s) sampling rates. With this approach, the transient absorption changes of the sample are recorded after pulsed laser excitation from nanoseconds to seconds at a preset frequency, typically at the beginning of the scanning range. Then, the frequency is changed in a stepwise manner (i.e., the wavenumber spacing), and the time traces are recorded at each frequency until the final frequency is reached. In the end, the time traces collected at each wavenumber of the frequency range are compiled to yield the matrix of time-resolved absorption changes, from which spectra are extracted by cutting along the spectral dimension. The smaller the wavenumber spacing, the more detailed the spectra will be, and also more time is invested for their collection.

In both setups, the photoexcitation of the protein was carried out by a pulsed ( $\Delta t = 10$  ns) Nd:YAG laser (Minilite II, Continuum), with parameters  $\lambda_{exc} = 532$  nm and  $E_{exc} = 3$  mJ/cm<sup>2</sup> (for single-shot experiments,  $E_{exc}$  was increased to 6.5 mJ/cm<sup>2</sup>). The data acquisition was synchronized to the Q-switched output of the excitation laser. The difference absorbance ( $\Delta A$ ) was calculated by using the mean intensity of the pretrigger points as background and applying  $\Delta A = -\log(I/I_{background})$ . Both datasets were logarithmically averaged along the time axis, reducing the number of points to 20 per decade for each wavenumber. The datasets were subjected to global exponential analysis to deduce the timings of maximal intermediate concentration (see Figs. S2–S4 in the [supplementary material](#)).

## Data denoising by lifetime density analysis

Time-resolved spectroscopic data can be modeled in most cases as a sum of exponentials. Such modeling is also a suitable way to remove noise not only along the temporal dimension but also along the spectral dimension. An advantage of a lifetime density analysis (LDA) of the time-resolved data over other fitting techniques (e.g., global exponential fitting) is its lower dependence on the assumed model. While global exponential fitting tries to model the data with a minimum number of pre-defined exponentials, LDA attempts to reproduce the measured data with a quasi-continuous set of time constants. Our LDA algorithm was implemented in Python and it is based on using augmented matrices and singular value decomposition (SVD), as introduced by the PyLDM package written by Dorlhiac *et al.*<sup>18</sup> Our source code is available at <https://github.com/deef128/trtoolbox>. Briefly, let  $\mathbf{D}$  be an  $n_t \times n_r$  matrix containing in its columns exponential decays ( $e^{-t/\tau}$ ) defined for  $n_t$  time values and  $n_r$  time constants. Furthermore, let  $\mathbf{A}$  be the recorded experimental data matrix of size  $n_t \times n_w$ , with  $n_w$  being the number of wavenumbers points.  $\mathbf{D}$  and  $\mathbf{A}$  will be related by (1),

$$\mathbf{A} = \mathbf{D} \cdot \mathbf{x} + \mathbf{E}, \quad (1)$$

where  $\mathbf{x}$  is an  $n_r$  vector with the amplitudes (pre-factors) of the exponentials, i.e., the lifetime density distribution, and  $\mathbf{E}$  is an  $n_t \times n_w$  matrix representing the unknown error (noise) in the data. To estimate  $\mathbf{x}$  from  $\mathbf{D}$  and  $\mathbf{A}$  in the presence of noise, we applied the Tikhonov regularization. This method combines a least-square minimization of the residual between the data and the model ( $\|\mathbf{A} - \mathbf{D} \cdot \mathbf{x}\|_2$ ) and the minimization of the two-norm of  $\mathbf{Lx}$ . This second component is introduced to punish large or rapidly changing values in the elements of  $\mathbf{x}$ , aiming to make  $\mathbf{x}$  as simple as possible. In this paper, we use the identity matrix for  $\mathbf{L}$ , which leads to the minimization of the two-norm of  $\mathbf{x}$ . Thus, we arrive to the minimization problem

$$\|\mathbf{A} - \mathbf{D} \cdot \mathbf{x}\|_2 + \alpha \|\mathbf{x}\|_2, \quad (2)$$

with  $\alpha$  being the regularization parameter—a scalar that sets the balance between best describing the experimental data (e.g., minimizing  $\|\mathbf{A} - \mathbf{D} \cdot \mathbf{x}\|_2$ ) and having a “simple” solution (e.g., minimizing  $\|\mathbf{x}\|_2$ ). Once solution  $\mathbf{x}$  is obtained, the estimated noiseless data are obtained as  $\mathbf{D} \cdot \mathbf{x}$ .

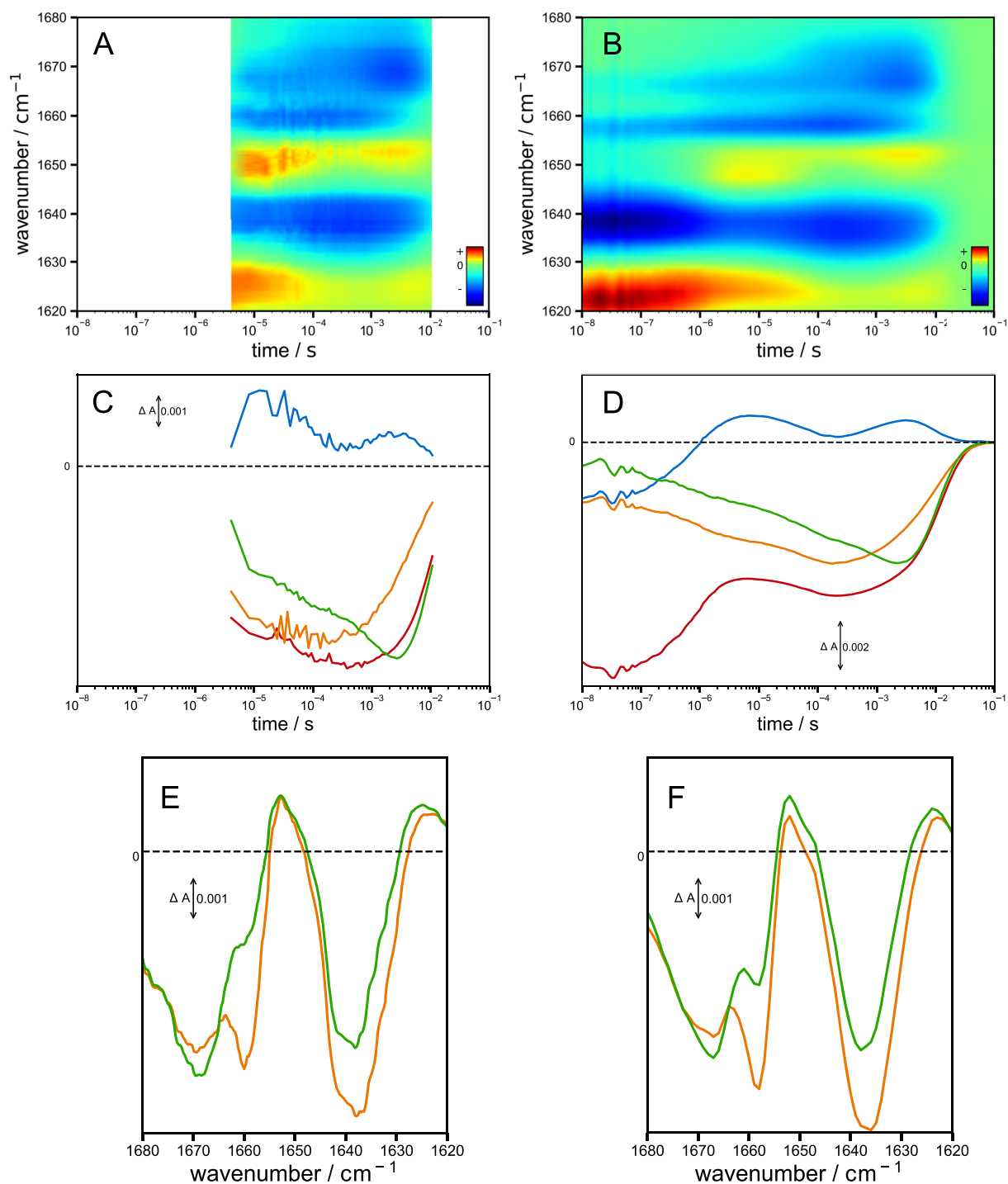


**FIG. 2.** Comparison of time-resolved IR absorption data of bacteriorhodopsin acquired by dual-comb spectroscopy (DCS) (left) and by a tunable external cavity quantum cascade laser (EC-QCL) setup (right) at a spectral resolution of  $4.5 \text{ cm}^{-1}$ . The dataset obtained by the QCL setup has been smoothed using a Savitzky–Golay filter to match the spectral resolution of the DCS data. (a) and (b) Contour plots covering the frequency range from 1680 to  $1620 \text{ cm}^{-1}$ . (c) and (d) Kinetic traces of the most prominent bands:  $1639 \text{ cm}^{-1}$  (red),  $1650 \text{ cm}^{-1}$  (blue),  $1660 \text{ cm}^{-1}$  (orange), and  $1670 \text{ cm}^{-1}$  (green). (e) and (f) Spectra at  $300 \mu\text{s}$  (orange) and at  $5.3 \text{ ms}$  (green) after pulsed light excitation, representative for the M and N/O intermediates, respectively. The datasets were acquired by averaging 3000 recordings with the DCS. The same number of total recordings resulted from 50 acquisitions at each wavenumber with  $1 \text{ cm}^{-1}$  spacing in the case of EC-QCL.

## RESULTS

## Comparison of time-resolved DCS and EC-QCL experiments in the amide I range

The frequency combs used in this study provide IR absorption data in the frequency range between 1680 and 1620  $\text{cm}^{-1}$  covering the amide I mode of the protein backbone. Although the EC-QCL is tunable across a broader spectral range, it was restricted in this study to match the DCS frequency range for direct comparison (Fig. 2). By spanning the time range from  $10^{-8}$  to  $10^{-1}$  s, the EC-QCL excels the time range of the DCS system ( $10^{-6}$  to  $10^{-2}$  s). While the time resolution of the EC-QCL setup is limited by the rise time of the detector, the time resolution of the DCS setup is ultimately determined by the difference in the repetition frequency of both frequency combs.<sup>10,12</sup> Due to the small linewidth of individual laser lines in both the setups as compared to the width of the vibrational bands in the condensed phase,<sup>10,19</sup> the effective spectral resolution (i.e., the ability to resolve two nearby bands) is actually limited by the wavenumber spacing (i.e., how many data points are measured per  $\text{cm}^{-1}$ ). The DCS yields spectra with an inherent spacing between the comb lines of about  $0.3 \text{ cm}^{-1}$ . Later, single comb lines are averaged to improve the SNR at the expense of the spectral resolution,<sup>12</sup> as described in the “Methods” section. Instead, the wavenumber spacing in the EC-QCL is not fixed but determined by how densely time traces are recorded along the spectral

dimension. In the present case, we recorded the time traces with a wavenumber spacing of  $1 \text{ cm}^{-1}$  (one data point per  $\text{cm}^{-1}$ ), which were later processed to provide the same spectral resolution as in the DCS experiments. Smaller spacings are possible but require more repetitions to cover a given spectral range.

Both datasets (Fig. 2) agree well and resemble already published FTIR data on bacteriorhodopsin recorded under similar conditions.<sup>20</sup> The negative band centered at  $1639 \text{ cm}^{-1}$  has been assigned to the C=N stretching vibration of the protonated retinal Schiff base of ground-state bR, which shifts to  $1624 \text{ cm}^{-1}$  upon deprotonation in the M intermediate.<sup>21</sup> Bands at  $1650$ ,  $1660$ , and  $1670 \text{ cm}^{-1}$  are associated with protein conformational changes as initially reported by low-temperature FTIR<sup>22</sup> and confirmed by time-resolved FTIR spectroscopy.<sup>15,20</sup> Changes in the amide I bands at  $1650$  and  $1670 \text{ cm}^{-1}$  are the largest upon formation of the N/O-intermediate. Based on previous FTIR results, this conformational change lowers the  $\text{pK}_a$  of D96 from higher than 12 down to 7.1,<sup>23</sup> thereby triggering proton transfer from D96 to the retinal Schiff base.<sup>20,22</sup>

## Time-resolved single-shot IR experiments to trace conformational changes in the protein backbone

We conducted single-shot experiments in the amide I range ( $1680\text{--}1620 \text{ cm}^{-1}$ ) to explore the option of probing irreversible

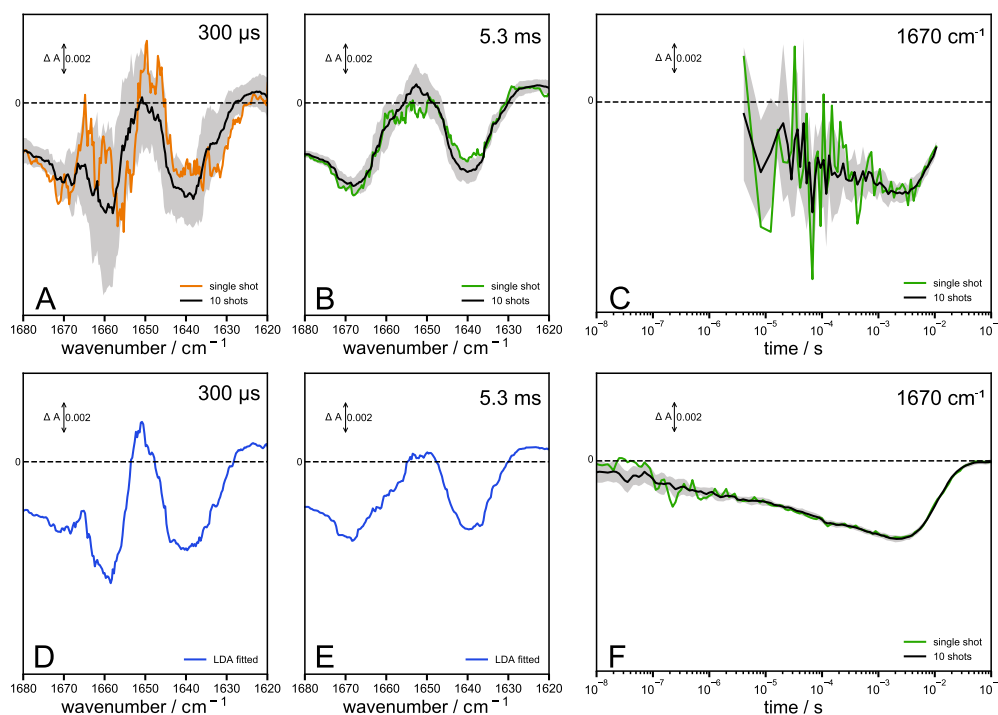


**FIG. 3.** Time-resolved single-shot experiments using dual-comb spectroscopy (DCS) [(a)–(e)] and external cavity quantum cascade laser (EC-QCL) spectroscopy (f). (a) and (b) Single-shot spectra recorded by DCS and extracted at  $300 \mu\text{s}$  and at  $5.3 \text{ ms}$ , respectively, after ns pulsed excitation. (c) and (f) Kinetic traces at  $1670 \text{ cm}^{-1}$  for DCS and EC-QCL, respectively. In panels (a)–(c) and (f), colored traces represent single-shot data, and black traces are the average of ten single-shot experiments. Gray shading displays the standard deviation determined from ten single-shot experiments ( $\Delta A_{10\text{shots}} \pm \sigma$ ). Panels (d) and (e) show the same single-shot spectra as in panels (a) and (b) but after applying the lifetime distribution analysis with  $\alpha = 9.78$  (blue trace). The DCS data are at a spectral resolution of  $8.1 \text{ cm}^{-1}$ .

reactions. The SNR in the kinetic experiments performed with the EC-QCL setup is sufficient to record time-resolved data from 10 ns to 100 ms, but at a single frequency only [Fig. 3(f)]. In this respect, DCS is superior as difference spectra can be recorded together with the kinetics even under single-shot conditions [Figs. 3(a)–3(e)]. Although the noise is considerably larger under single-shot conditions, the spectral features of the bR photocycle are resolved by DCS [Figs. 3(a) and 3(b)]. The SNR is higher in the spectrum at 5.3 ms than at 300  $\mu$ s due to the noise reduction resulting from logarithmic averaging on the time axis [Fig. S1(B) in the [supplementary material](#)], which is also evident from the kinetic trace recorded at 1670  $\text{cm}^{-1}$  [Fig. 3(c)]. The comparison of the single-shot and ten-shot spectrum at 5.3 ms after pulsed excitation [Fig. 3(b)] reveals high similarity between the two. However, spectra at 300  $\mu$ s are clearly different in single-shot and ten-shot recordings [Fig. 3(a)]. Applying the lifetime density analysis (LDA) to the single-shot spectra improved its SNR, such that all spectral features are resolved and match the average of ten shots [Figs. 3(d) and 3(e)]. As can be discerned from the standard deviation of the averaged experiments [Figs. 3(a) and 3(b)], the noise is dependent on the frequency, which is mainly due to the inhomogeneous power distribution of the frequency comb and of the absorbance of the sample. The spectral noise dependence is also inferred from the noise

distribution calculated from the standard deviation of the pretrigger data points [see Fig. S1(A) in the [supplementary material](#)]. Comparing the kinetic traces of single-shot DCS and EC-QCL experiments [Figs. 3(c) and 3(f)], the noise is considerably lower in the latter. This observation can be explained by the fact that the EC-QCL setup has a higher emission power per wavenumber as compared to the DCS.

### Proton transfer reactions revealed in a single-shot TR-IR experiment

Another laser module was used to conduct experiments in the frequency range between 1770 and 1720  $\text{cm}^{-1}$  for probing protonation events of single aspartic acids by a single shot. Because signals from protonation changes of single carboxylic acid residues are usually much weaker than absorption changes of vibrational bands of the peptidic amide group or from cofactors, a method with high SNR is particularly relevant. The weaker background absorption in this spectral region (1770–1720  $\text{cm}^{-1}$ ) compared to the amide I region (1680–1620  $\text{cm}^{-1}$ ), where the absorption of the peptide backbone and the water bending mode overlap, allows us to use thicker samples, which increase the changes in absorbance and leads to sufficient SNR. As demonstrated in Figs. 4(a)–4(d), a single shot is sufficient to extract the spectro-temporal features assigned to the protonation

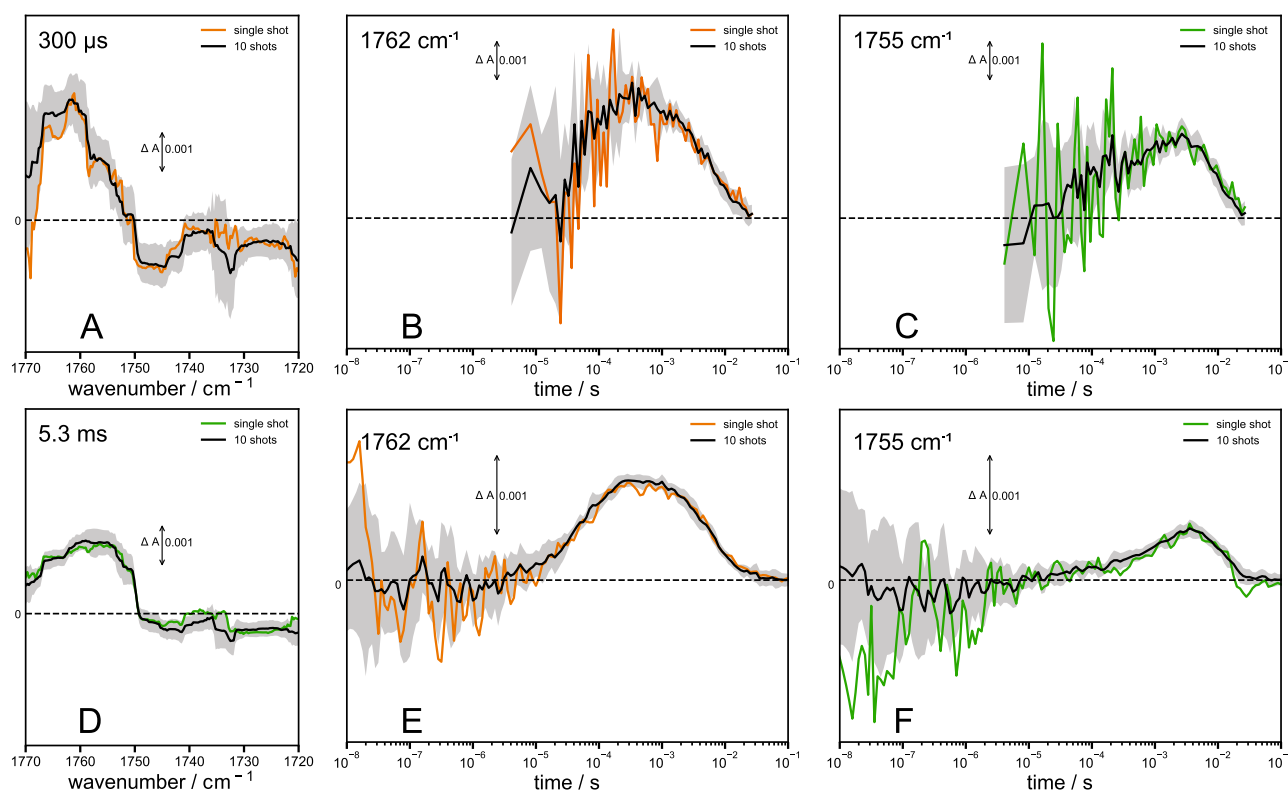


**FIG. 4.** Probing protonation dynamics of the counter ion D85 in bacteriorhodopsin by dual-comb spectroscopy (DCS). (a) and (d) M- and N/O like spectra by DCS, extracted at 300  $\mu$ s and 5.3 ms, respectively. (b) and (c) Kinetics at 1762 and 1755  $\text{cm}^{-1}$ , respectively, by DCS. (e) and (f) Kinetics at 1762 and 1755  $\text{cm}^{-1}$ , respectively, by external cavity quantum-cascade laser setup (EC-QCL). Colored traces are obtained by a single shot, black traces are the average of ten single-shot experiments, and the gray shading displays the standard deviation determined from ten single-shot experiments ( $\Delta A_{10\text{shots}} \pm \sigma$ ). The DCS data are shown with 8.1  $\text{cm}^{-1}$  spectral resolution.

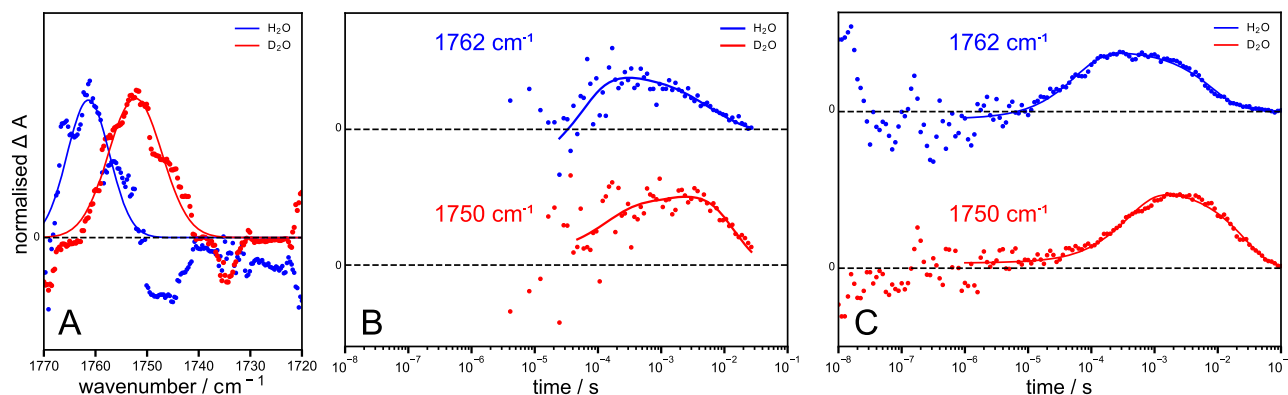


**FIG. 5.** Elucidation of spectral and kinetic isotope effects by single-shot experiments. (a) M intermediate spectra of bR in H<sub>2</sub>O at 300  $\mu$ s (blue) and in D<sub>2</sub>O at 1.2 ms (red). (b) and (c) Single-shot kinetics in H<sub>2</sub>O (blue, 1762  $\text{cm}^{-1}$ ) and D<sub>2</sub>O (red, 1750  $\text{cm}^{-1}$ ) obtained by dual-comb spectroscopy (DCS) and external cavity quantum-cascade laser setup (EC-QCL), respectively. Points show the raw data, the lines represent Gaussian fits for spectra (a), and (global) exponential fits for kinetics (b) and (c). The DCS data are shown with 8.1  $\text{cm}^{-1}$  spectral resolution.

of D85. The obtained kinetics in single-shot experiments are noisy but still informative [Figs. 4(b) and 4(c)], while the same kinetics obtained by our EC-QCL setup outmatch them in terms of SNR and time resolution [Figs. 4(e) and 4(f)].

We applied global exponential analysis and kinetic modeling to the DCS datasets acquired in a single shot and by averaging ten shots (Figs. S3 and S4 in the [supplementary material](#)), illustrating that the data quality in a single shot is sufficient to extract the same information on intermediate states as in a ten-shot experiment.

To survey our single-shot experiments, we exchanged dissociable protons for deuterons by incubation of the sample in D<sub>2</sub>O, and determined the vibrational and kinetic isotope effects. H/D exchange at functionally relevant amino acid residues affects the photocycle of bR by slowing down proton transfer steps (kinetic isotope effect). The frequency of the C=O stretching vibration of D85 shifts down by about 10  $\text{cm}^{-1}$ , which is due to the vibrational isotope effect.<sup>24</sup> Both of our QCL-based methods are able to resolve the aforementioned kinetic isotope effect in single-shot experiments. As already discussed, the kinetics obtained by the EC-QCL setup surpass those from DCS, both in terms of SNR and time resolution [Figs. 5(b) and 5(c)]. However, only DCS is able to spectrally resolve the vibrational isotope effect of D85 in a one-shot acquisition [Fig. 5(a)], demonstrating its suitability to probe non-repetitive reactions in the future by recording spectro-temporal data in a single-shot experiment.

## DISCUSSION

We have examined the applicability of two different QCL-based time-resolved IR absorption spectroscopic techniques to probe conformational and protonation dynamics in proteins. With the photoactivated proton pump bR as a model system in hand, where protein conformational changes enable proton translocation across the biological membrane,<sup>20,25</sup> we highlighted QCL-based IR absorption spectroscopy as a powerful tool to investigate structure–function relationships in proteins. The DCS and the EC-QCL techniques take advantage of the high emission power of QCLs permitting to probe

longer optical pathlengths to achieve higher SNR, as well as proteins in solution or even protein-crystals.<sup>10,26</sup>

Both QCL-based setups provided time-resolved data in single-shot experiments demonstrating the possibility to probe irreversible reactions but with notable differences between them. Although the EC-QCL setup is capable to record single time traces from single-shot experiments at a much higher SNR than the DCS does [Figs. 3(f), 4(e), and 4(f)], it does not provide any spectral range. On the contrary, the DCS setup is capable of recording spectro-temporal data in a single recording. This is the key advantage of DCS over EC-QCL, as it allows us to apply data analysis tools, such as global analysis or LDA, to extract both kinetic and spectral information, making it possible to derive reaction schemes from even single-shot experiments. On the other hand, the EC-QCL setup excels DCS both in its temporal resolution (ns vs  $\mu$ s) and in the covered time range ( $\sim$ 100 ms vs  $\sim$ 20 ms). Indeed, the temporal dimension of DCS in this study is limited to the range of 4  $\mu$ s to 26 ms. An improved time resolution of 320 ns has been reported for DCS,<sup>12</sup> and a novel acquisition scheme has been introduced recently, extending the time range of the DCS setup to minutes.<sup>13</sup>

Our analysis shows that the noise in DCS decreases with time upon logarithmic averaging, just as expected for random noise [Figs. S1(B) and S1(D) in the [supplementary material](#)]. In comparison, time-resolved step-scan FTIR spectroscopy shows an initial reduction of the noise with time, but the noise increases in the millisecond time range from non-random errors caused by instabilities of the movable mirror of the interferometer.<sup>27</sup> Similarly, our EC-QCL setup shows a reduction in the noise with time but suffers from non-random errors at times longer than 100 ms caused by instabilities in emission intensity of the QCL. Therefore, our homebuilt EC-QCL setup could benefit from adding a second MCT detector for referencing, as it is used in DCS, allowing to reliably extend the time range beyond 100 ms up to several seconds.

In terms of the spectral coverage, DCS is so far limited to  $\sim$ 60  $\text{cm}^{-1}$  per laser module, which represents a serious limitation for spectroscopic analysis. In comparison, our EC-QCL allows a

spectral range of  $\sim 150\text{ cm}^{-1}$  for one laser and a recently reported setup based on only four tunable QCLs allows for an almost gapless tuning range between 2250 and  $1150\text{ cm}^{-1}$ .<sup>28</sup> Another important aspect to consider is the spectral resolution. In both EC-QCL and step-scan FTIR spectroscopy, the spectral resolution can only be improved by an increased experimental effort. With the EC-QCL, the emission frequency is tuned by the grating in such a way that recording twice as many emission frequencies is required to improve the spectral resolution by a factor of two. In a step-scanning interferometer, the optical pathlength difference of the movable mirror needs to be extended. Thereby, twice the number of optical pathlength differences correspond to  $2\times$  higher spectral resolution. As a result, the number of repeated experiments is doubled in both techniques. In contrast, DCS inherently provides a high spectral resolution without any additional experimental effort. However, it is noted that adjacent comb lines are often averaged to increase the SNR at the expense of the spectral resolution. Also, spectral averaging needs to be performed by a weighted moving average due to the uneven noise distribution in DCS. This type of averaging, in some cases, may lead to distortions in the shapes of spectral bands, which is evident from the single- and ten-shot data presented in Figs. 4(a) and 4(d).

In summary, we have demonstrated that the temporal evolution of vibrational spectral changes in proteins can be recorded in a single-shot experiment by dual-comb spectroscopy. Time-resolved experiments on slow or non-cycling photoreceptors, such as blue-light photoreceptors<sup>30</sup> or visual rhodopsins<sup>29</sup> or even light-insensitive proteins, will be facilitated by the possibility of single-shot measurements in combination with techniques such as caged compounds or flow cells.<sup>13,31</sup> Such experiments can complement x-ray serial crystallographic experiments using free electron lasers (FEL), which is a single-shot technique. Here, time-resolved IR spectroscopy provides valuable information to guide data acquisition and interpret structural data.<sup>26</sup> Moreover, the proceedings of the molecular mechanisms of irreversible reactions, which represent the vast majority of transformations in biology and chemistry, can be traced and elucidated with the presented approaches.

## SUPPLEMENTARY MATERIAL

See the [supplementary material](#) for further details on noise distribution and fitting procedures.

## ACKNOWLEDGMENTS

Technical support by Raphael Horvath and Markus Mangold (IRSweep, Staefa, Switzerland) is greatly appreciated. We thank Kirsten Hoffmann, Dorothea Heinrich, and Ramona Schlesinger (Genetic Biophysics, FU Berlin) for providing bR samples. L.S. acknowledges the support from the International Max Planck Research School (IMPRS) on Multiscale Bio-Systems. V.A.L.-F. acknowledges the support from the Ministerio de Ciencia e Innovación (MICINN)—Agencia Estatal de Investigación (AEI) (Grant No. PID2019-106103GB-I00). This work was funded by the German Research Foundation [Grant Nos. EXC 2008/1 (UniSysCat) and 390540038] and by SFB 1078, Project Nos. A1 and B3.

## AUTHOR DECLARATIONS

### Conflict of Interest

The authors have no conflicts to disclose.

## DATA AVAILABILITY

The data that support the findings of this study are available from the corresponding author upon reasonable request.

## REFERENCES

1. I. N. Serdyuk, N. R. Zaccai, and J. Zaccai, *Methods in Molecular Biophysics* (Cambridge University Press, 2017).
2. F. Siebert and P. Hildebrandt, *Vibrational Spectroscopy in Life Science* (John Wiley & Sons, 2008).
3. W. Uhmann, A. Becker, C. Taran, and F. Siebert, *Appl. Spectrosc.* **45**, 390 (1991).
4. T. Kottke, V. A. Lórenz-Fonfría, and J. Heberle, *J. Phys. Chem. B* **121**, 335 (2017).
5. V. A. Lórenz-Fonfría, *Chem. Rev.* **120**, 3466 (2020).
6. B. Süß, F. Ringleb, and J. Heberle, *Rev. Sci. Instrum.* **87**, 063113 (2016).
7. G. M. Greetham, P. M. Donaldson, C. Nation, I. V. Sazanovich, I. P. Clark, D. J. Shaw, A. W. Parker, and M. Towrie, *Appl. Spectrosc.* **70**, 645 (2016).
8. G. M. Greetham, D. Sole, I. P. Clark, A. W. Parker, M. R. Pollard, and M. Towrie, *Rev. Sci. Instrum.* **83**, 103107 (2012).
9. E. Ritter, L. Puskar, S. Y. Kim, J. H. Park, K. P. Hofmann, F. Bartl, P. Hegemann, and U. Schade, *J. Phys. Chem. Lett.* **10**, 7672 (2019).
10. B.-J. Schultz, H. Mohrmann, V. A. Lorenz-Fonfría, and J. Heberle, *Spectrochim. Acta, Part A* **188**, 666 (2018).
11. G. Villares, A. Hugi, S. Blaser, and J. Faist, *Nat. Commun.* **5**, 5192 (2014).
12. J. L. Klocke, M. Mangold, P. Allmendinger, A. Hugi, M. Geiser, P. Jouy, J. Faist, and T. Kottke, *Anal. Chem.* **90**, 10494 (2018).
13. M. J. Norahan, R. Horvath, N. Woitzik, P. Jouy, F. Eigenmann, K. Gerwert, and C. Köttling, *Anal. Chem.* **93**, 6779 (2021).
14. I. Radu, M. Schlegler, C. Bolwien, and J. Heberle, *Photochem. Photobiol. Sci.* **8**, 1517 (2009).
15. M. S. Braiman, O. Bousché, and K. J. Rothschild, *Proc. Natl. Acad. Sci. U. S. A.* **88**, 2388 (1991).
16. K. Gerwert, B. Hess, J. Soppa, and D. Oesterheld, *Proc. Natl. Acad. Sci. U. S. A.* **86**, 4943 (1989).
17. M. Stauffer, S. Hirschi, Z. Ucurum, D. Harder, R. Schlesinger, and D. Fotiadis, *Methods Protoc.* **3**, 51 (2020).
18. G. F. Dorliac, C. Fare, and J. J. van Thor, *PLoS Comput. Biol.* **13**, e1005528 (2017).
19. U. Szczepaniak, S. H. Schneider, R. Horvath, J. Kozuch, and M. Geiser, *Appl. Spectrosc.* **74**, 347 (2019).
20. G. Souvignier and K. Gerwert, *Biophys. J.* **63**, 1393 (1992).
21. K. Bagley, G. Dollinger, L. Eisenstein, A. K. Singh, and L. Zimányi, *Proc. Natl. Acad. Sci. U. S. A.* **79**, 4972 (1982).
22. P. Ormos, *Proc. Natl. Acad. Sci. U. S. A.* **88**, 473 (1991).
23. C. Zscherp, R. Schlesinger, J. Tittor, D. Oesterheld, and J. Heberle, *Proc. Natl. Acad. Sci. U. S. A.* **96**, 5498 (1999).
24. T. Resler, B.-J. Schultz, V. A. Lórenz-Fonfría, R. Schlesinger, and J. Heberle, *Biophys. J.* **109**, 287 (2015).
25. T. Weinert, P. Skopintsev, D. James, F. Dworkowski, E. Panepucci, D. Kekilli, A. Furrer, S. Brünle, S. Mous, D. Ozerov, P. Nogly, M. Wang, and J. Standfuss, *Science* **365**, 61 (2019).

- <sup>26</sup>P. Skopintsev, D. Ehrenberg, T. Weinert, D. James, R. K. Kar, P. J. M. Johnson, D. Ozerov, A. Furrer, I. Martiel, F. Dworkowski, K. Nass, G. Knopp, C. Cirelli, C. Arrell, D. Gashi, S. Mous, M. Wranik, T. Gruhl, D. Kekilli, S. Brünle, X. Deupi, G. F. X. Schertler, R. M. Benoit, V. Panneels, P. Nogly, I. Schapiro, C. Milne, J. Heberle, and J. Standfuss, *Nature* **583**, 314 (2020).
- <sup>27</sup>C. Rödiger and F. Siebert, *Appl. Spectrosc.* **53**, 893 (1999).
- <sup>28</sup>P. Stritt, M. Jawurek, and K. Hauser, *Biomed. Spectrosc. Imaging* **9**, 55 (2020).
- <sup>29</sup>R. Vogel and F. Siebert, *Biopolymers* **72**, 133 (2003).
- <sup>30</sup>T. Kottke, A. Xie, D. S. Larsen, and W. D. Hoff, *Annu. Rev. Biophys.* **47**, 291 (2018).
- <sup>31</sup>J. L. Klocke and T. Kottke, *Phys. Chem. Chem. Phys.* **22**, 26459 (2020).